Assessing CCS Capillary Trapping Capacity of Ivar Aasen field Through Steady State Supercritical CO_2-Brine Relative Permeability Measurements at Reservoir Conditions

Nasiru Abiodun Idowu[1,*], Egil Boye Petersen[2], Gunn Anita Løvrød[1], Trond Laxåbakk Danielsen[1] and Arne Johan Førnes[1]

[1]Stratum Reservoir, Trondheim, Norway
[2]AkerBP Stavanger, Norway

Abstract. Capillary trapping is a critical mechanism for long-term CO_2 storage security. Reliable supercritical CO_2–brine ($scCO_2$–B) relative permeability data under reservoir conditions is essential to quantify residual trapping and assess candidate formations for CCS. We present results of steady-state $scCO_2$–B imbibition experiments on Ivar Aasen sandstone cores—an analogue for potential storage sites—at reservoir conditions (69 °C, 193 bar) using equilibrated fluids and in-situ saturation monitoring (ISSM). There was a considerable brine imbibition at the first water fraction (F_w) of 0.02 and very little imbibition thereafter resulting in about 0.36 fraction of pore volume (FPV) trapped CO_2. The end-point brine relative permeability was less than 0.1, confirming strongly water-wet behaviour. While this trapped saturation remained stable after injecting about 10 PV of brine at F_w of 1.0, achieving full steady-state stability (in the differential pressure data and ISSM data) required more than 2,160 PV and progressively stripped the trapped CO_2 — an artefact of excessive throughput rather than true reservoir behaviour. We therefore recommend limiting the total PV of injected brine at F_w of 1.0 and during the bump flow to a maximum of 5 PV to preserve physically meaningful residuals when performing similar laboratory experiments. Secondary drainage and secondary imbibition relative permeability were measured to assess hysteresis. History matching the measured pressure and production data shows a very good agreement with the simulated data and corroborates the trapping capacity. These findings demonstrate Ivar Aasen's suitability as a CCS analogue and provide practical guidance for designing reliable laboratory workflows.

1 Introduction

Norwegian carbon capture and storage (NCCS) research and world-wide CCS projects require reliable multiphase transport properties – capillary pressure and relative permeability data - at reservoir conditions to evaluate and assess the capillary trapping capacity of potential sites and their suitability for CO_2 sequestration. A review paper summarising relative permeability experiments for 22 sandstones and 13 carbonates from several Canadian sites published by Stefan Bachu [1] concluded that "the relative permeability displacement characteristics of CO_2 – brine systems at in-situ conditions are highly site specific, depending most likely of rock fabric, structure and wettability, and cannot be predicted based on any other commonly measured rock characteristics such as pore characteristics, porosity and absolute permeability".

However, there is a scarcity of relative permeability data for many potential geographical sites due to costs and extensive time required for laboratory measurements [2]. Besides, most of the published relative permeability data is the drainage cycle of the CO_2 – brine tests [3 - 11] and in some cases unsteady state experiments were carried out to quantify trapped $scCO_2$ saturation thereafter [6, 10]. This introduces uncertainties and a recent study has shown "that uncertainty in key relative-permeability parameters, particularly CO_2 endpoint relative permeability, initial water saturation, residual gas saturation, and Corey exponents, exerts a first-order control on CO_2 plume geometry, trapping efficiency, and long-term storage security" [12].

Besides capillary trapping, there are three other main trapping mechanisms that contribute to the overall security of the injected CO_2 at any given site or region. These mechanisms [13] are: (1) Structural trapping – where the buoyant, $scCO_2$ rises through the porous rocks and is trapped by an impermeable caprock layer. (2) Dissolution or solubility trapping where the $scCO_2$ dissolves in brine. So, the brine becomes denser and sinks to the bottom thereby reducing the risk of migrating back to the surface. (3) Mineral trapping where the dissolved scCO2 forms a weak carbonic acid which reacts thereafter with surrounding minerals in the rock to form solid carbonate minerals. **Fig. 1** depicts the different trapping mechanisms [14].

This study focuses on capillary trapping and the main objectives are (1) to measure imbibition, secondary drainage and secondary imbibition steady-state relative permeability starting from a representative initial water saturation established by the porous plate method on sandstone samples from the Ivar Aasen field - **Fig. 2** and

* Corresponding author: nasiru.idowu@stratumreservoir.com

(2) assess its suitability as a CCS analogue. We verify and validate the measured trapping efficiency by history matching the experimental pressure and production data. Finally, we highlight inherent laboratory artefacts and provide practical guidance to overcome these when performing similar experiments. It is our view that this is the first published experimental study to provide a complete steady-state relative permeability data set for imbibition, secondary drainage and secondary imbibition at reservoir conditions in sandstone cores.

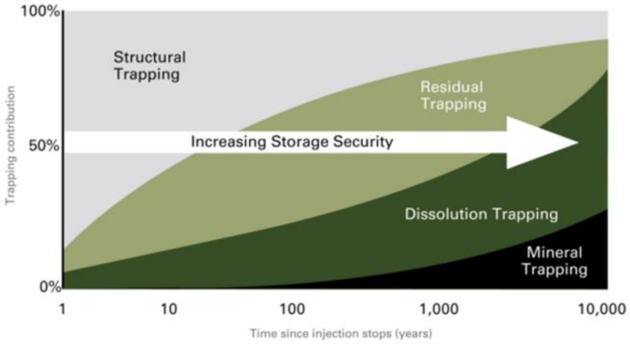

Fig. 1. Trapping mechanisms and storage security [14].

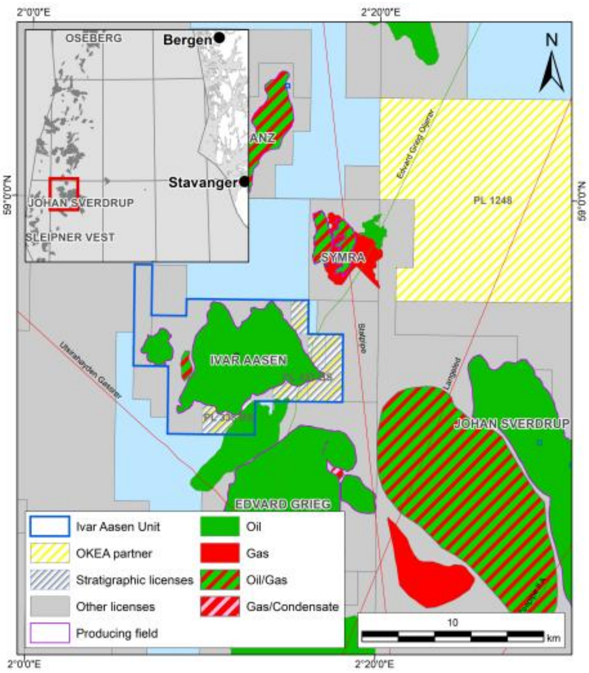

Fig. 2. Location of Ivar Aasen field in the North Sea [15].

2 Materials and Methods / Methodology

2.1 Plug Samples

Two plug samples from Ivar Aasen field were used in this study. Helical CT scan results show the presence of high-density minerals in both samples. However, sample #1 seems homogeneous while sample #2 exhibits weak laminations as shown in **Fig. 3**. X-ray diffraction analysis showed that the cores contained approximately 5 wt% clay minerals including illite, mica, kaolinite, etc - **Fig. 4**. Therefore, an immersed Soxhlet cleaning method and critical point drying (CPD) with CO_2 were used to preserve the clay minerals.

The CPD method involves the following steps as shown in **Fig. 5**:

- Flooding the plug with methanol at temperature and pore pressure indicated as Point #1 on the phase diagram while maintaining net confining pressure (NCP).
- Reducing the temperature (to < 31.1°C) while maintaining both pore pressure and NCP to Point #2.
- Displacing the methanol with CO_2 while maintaining pore pressure and NCP.
- Increasing the temperature to ≥ 35 °C while maintaining pore pressure and NCP – Point #3.
- Reducing the pore pressure to atmospheric while maintain NCP by reducing overburden pressure.
- Finally, reducing the temperature to ambient conditions.

Basic petrophysical properties were subsequently measured and the initial water saturation (S_{wi}) was established using the gas/water porous plate method at a maximum drainage capillary pressure of 15 bar. The Klinkenberg gas permeability (K_L), absolute water permeability and effective gas permeability at S_{wi} ($K_g(S_{wi})$) were measured at 25 bar net confining pressure (NCP). Table 1 summarizes the dimensions and basic petrophysical properties of the two plug samples.

Since sample #1 appeared homogeneous and exhibited porosity and S_{wi} values similar to sample #2, it was selected for the steady-state relative permeability measurements.

2.2 Fluids

To enhance the contrast between the synthetic formation water (SFW) and $scCO_2$ during γ-ray in-situ saturation monitoring (ISSM), the SFW was doped with cesium chloride (CsCl). When preparing the doped SFW (dSFW), the NaCl concentration of the SFW was adjusted to match the ionic strength of the original SFW. Thus, the addition of dopant should not change the plug samples wettability, and the samples were not exposed to crude oil during the tests. Table 2 summarizes the properties of the dSFW and the $scCO_2$ at reservoir test conditions while **Fig. 5** shows the CO_2 phase diagram. It (**Fig. 5**) confirms that the CO_2 is in a supercritical state ($scCO_2$) at these conditions.

The dSFW and $scCO_2$ were recirculated until the fluids were in equilibrium at test conditions. The plug sample was flooded with 5 pore volumes of humidified / equilibrated $scCO_2$ to displace the nitrogen gas used to establish S_{wi}. Following this, the effective $scCO_2$ permeability at initial water saturation - $k_{CO_2}(S_{wi})$ was measured. At 103 bar and 25 bar NCP, $k_{CO_2}(S_{wi})$ and $K_g(S_{wi})$ were 169 mD and 194 mD respectively. $k_{CO_2}(S_{wi})$ was used as the base permeability for calculating the imbibition relative permeability.

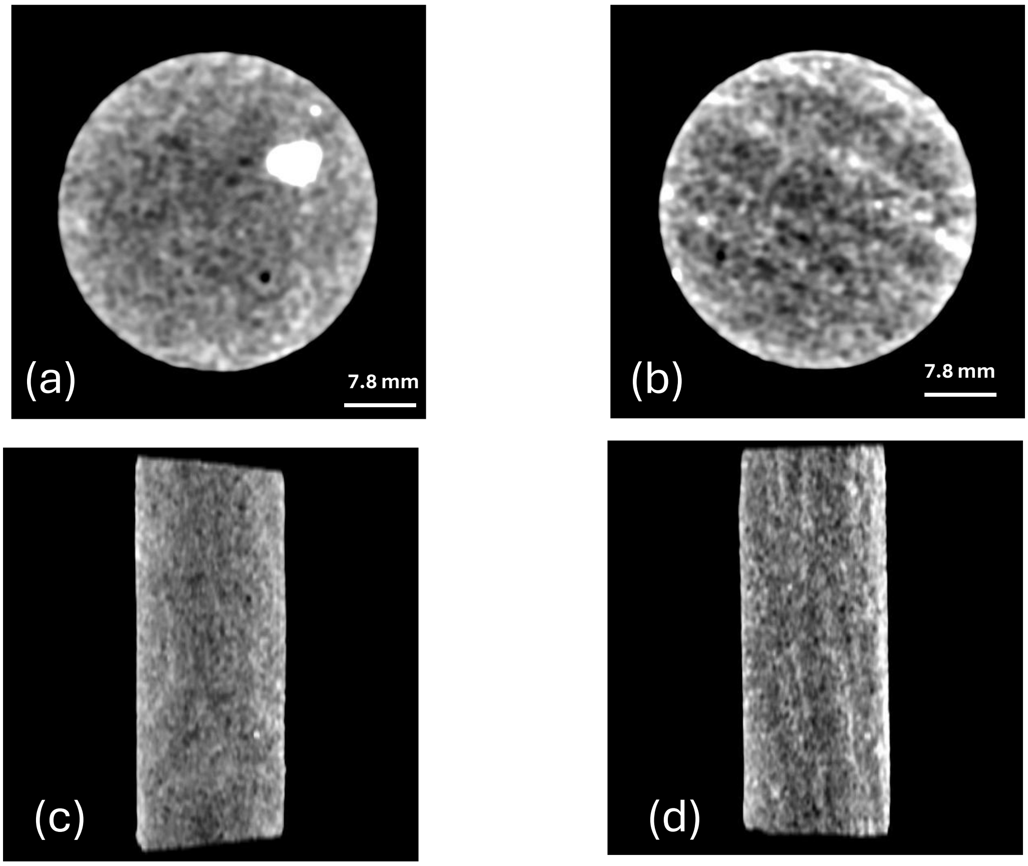

Fig. 3. Cross sectional and longitudinal CT images of Sample #1 (a and c) and Sample #2 (b and d).

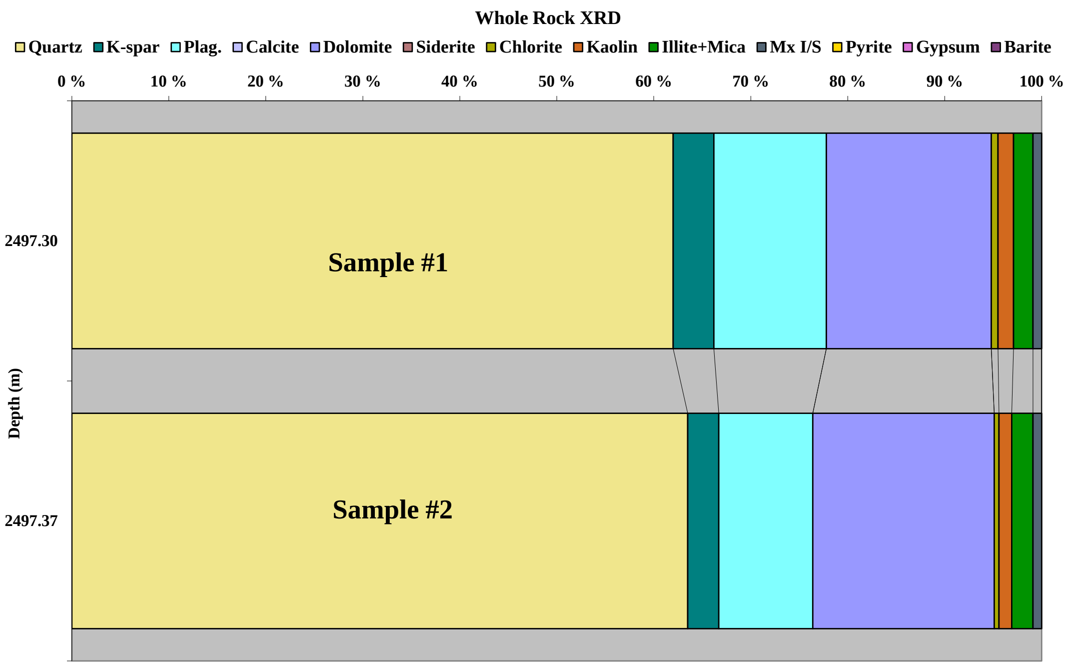

Fig. 4. Whole core X-ray diffraction analysis results.

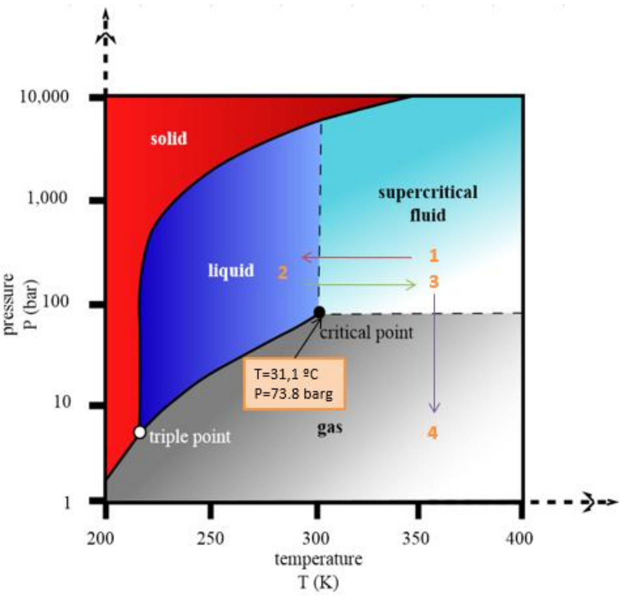

Fig. 5. CO_2 pressure-temperature phase diagram [16].

Table 1. Summary of basic petrophysical properties.

Sample	#1	#2
Length (cm)	6.49	6.92
Diameter (cm)	3.76	3.77
Grain Density (g/ml)	2.66	2.66
Pore volume (ml)	15.92	16.77
Porosity (frac.)	0.222	0.219
Klinkenberg, K_L (mD)	171	402
Absolute water perm, K_w (mD)	154	361
S_{wi} – porous plate	0.203	0.195
$K_g(S_{wi})$	194	425

Table 2. $scCO_2$-brine fluid properties at test conditions.

Parameters	dSFW	$scCO_2$
Viscosity (cP)	0.440	0.051
Density (g/ml)	1.006	0.651
Temperature (°C)	69	
Pore pressure (bar)	193	
Net confining pressure (bar)	103	

2.3 Relative permeability measurements

A simplified schematic of the apparatus used for the measurements, with γ-ray ISSM and recirculating fluids to maintain equilibrium, is shown in **Fig. 6**. The flooding rig was equipped with heated, high precision Quizix pumps for injection of equilibrated fluids. Core holder, valve cabinets, separators and all lines were heated.

The imbibition relative permeability measurements were conducted at a constant flow rate with six (6) intermediate water fractions (F_w) and one (1) bump flood. To ensure gravity stable injection/displacement, the core holder was oriented vertically and the equilibrated dSFW and $scCO_2$ were injected from the bottom of the plug sample. At the end of the 100% fractional water flow, $k_w(Sco_2r)$ was measured using a multi-rate (four-point) measurement to ensure consistency and reliability of the measured data. A bump flood was subsequently performed, after which a new $kw(Sco_{2r,\ bump})$ was measured.

On completion of the imbibition relative permeability measurements, the injection/flow direction was reversed from the bottom to the top for the secondary drainage tests. The effective brine permeability at residual / trapped $scCO_2$ saturation - $k_w(Sco_{2r})$ was remeasured using the four-point measurement procedure. This value was used as the base permeability for calculating the secondary drainage relative permeability values at five (5) intermediate $scCO_2$ fractions (F_g).

At the end of the 100% F_g step, the effective $scCO_2$ permeability $kco2(S_{wr})$ was measured using the four-point measurement procedure. A bump flood was subsequently performed, after which a new multi-rate $kco_2(S_{wr,\ bump})$ was measured.

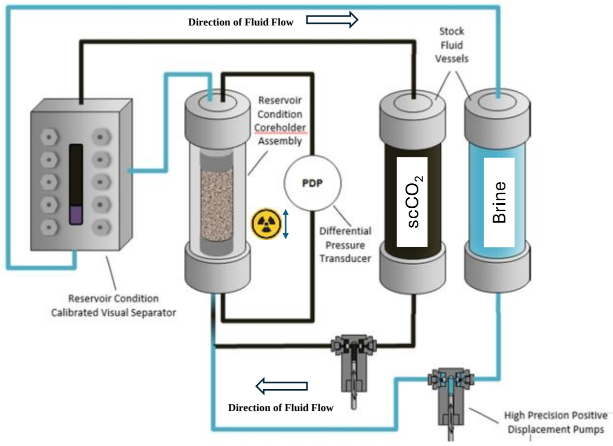

Fig. 6. Schematic of the apparatus used for the relative permeability measurements, showing flooding from bottom to top.

The secondary imbibition relative permeability measurements were started thereafter by changing the injection/flow direction from the top to the bottom of the plug sample again. The effective $scCO_2$ permeability $kco_2(S_{wirr})$ was remeasured. At the end of the five (5) intermediate F_w steps and 100% F_w step, a multi-rate $k_w(Sco_{2r})$ was measured. A bump flood was then performed, after which a new $k_w(Sco_{2r,\ bump})$ was obtained.

2.4 In-situ saturation monitoring (ISSM)

Gamma-ray scans were collected throughout the imbibition, secondary drainage and secondary imbibition tests at each fractional flow step, at 100% flooding and during bump floods. A minimum of the last six stable gamma scans were used for ISSM calculations at each step. However, it should be noted that the computation of the actual ISSM saturations could only be done after the acquisition of the equilibrated fluids reference scans at the end of the secondary imbibition measurements.

At the end of the secondary imbibition test, Karl Fischer (KF) titration was performed for saturation quality control. The plug sample was cleaned after the KF and thereafter fully (100%) saturated with equilibrated dSFW by miscible displacement of methanol.

The following steps were taken to obtain dSFW, $scCO_2$ and dry reference scans.

- When stable gamma scans were obtained, the 100% dSFW saturated reference scans were acquired and absolute water permeability (K_w) measured.
- The core was then flooded with 3 PV of Methanol.
- The core temperature was reduced to 25 °C while the pore pressure and the NCP were maintained.
- The core was subsequently flooded with 5 PV of liquid CO_2 to displace the methanol.
- The core temperature was increased back to the test temperature (69 °C).
- $scCO_2$ reference scans were then acquired.
- The pore pressure was reduced to atmospheric pressure while maintaining the NCP.
- The temperature was reduced to ambient temperature.
- Dry reference scans were then acquired for porosity computation.
- KL and helium PV were then measured at the test NCP.

3 Experimental results, simulations and discussions

By definition, primary drainage is the initial injection of a non-wetting fluid (oil, gas, or CO_2), into a rock sample that is fully saturated with water. Imbibition is the spontaneous absorption or forced injection of a wetting phase (water or oil) into a rock sample thereby displacing the non-wetting fluid.

Secondary drainage is the spontaneous absorption or forced injection of a non-wetting phase (oil, gas, or CO_2), into a rock sample that is partially saturated with water (after the first imbibition). Secondary imbibition is the spontaneous absorption or forced injection of a wetting phase (water or oil) into a rock sample subsequently displacing the non-wetting fluid after secondary drainage.

3.1 Imbibition results

The injection rates, water fractional flows, water saturations, injected volumes, as well as production and pressure data, water saturation profiles and measured imbibition relative permeability curves are presented in Table 3, **Fig. 7** and **Fig. 8**. There was a pore volume squeeze of 0.04 ml when the NCP was increased from 25 bar to 103 bar suggesting that the sample was well consolidated. To remove end-effects from the ISSM data, fluid saturations were computed from 0.092 to 0.955 length fraction of the sample. The measured ISSM S_{wi} was 0.229.

The water saturation profiles in **Fig. 7** – shows a considerable spontaneous brine imbibition at the first F_w of 0.02 (water flow rate of 0.16 ml/min) resulting in ISSM S_w of 0.562. From the second to the sixth F_w (F_w = 0.09 and 0.99 respectively), the ISSM S_w increased to 0.634. Consequently, injection of both mutually equilibrated $scCO_2$ and brine together from F_w of 0.02 to 0.99 resulted in a $scCO_2$ capillary trapping (Sco_{2r}) of 0.366 fraction of pore volume (FPV).

The Sco_{2r} remained unchanged after injecting 10 PV of brine at F_w = 1.0, although full steady-state stability had not yet been achieved. A total of 2,166 PV of brine injection was required to reach stability in both the differential pressure (dP) and ISSM data at F_w = 1.0 and progressively stripped the trapped $scCO_2$.

Full steady-state stability is defined quantitatively and qualitatively. When the average ISSM data over the entire plug sample remains within +/- one ISSM count for at least the last six ISSM data, quantitative stability is achieved. If the differential pressure (dP) visually remains/appears stable and unchanging, qualitative stability is achieved. When these two conditions are met simultaneously, full steady-state stability is achieved.

The total flow rate was reduced from 8.0 ml/min to 4.0 ml/min from the third water fraction onward to ensure that the dP remained well below 5% of the pore pressure [18]. The bump flood flow rate was 10 ml/min, and 828 PV of brine injection was required to reach stability.

3.2 Secondary drainage and imbibition results

The secondary drainage relative permeability results are presented in Table 4, **Fig. 9** and **Fig. 10**. The water saturation profiles show S_w decreasing from 1.0 to 0.688 at the first Fco_2 = 0.015 (gas flow rate of 0.06 ml/min). From the second to the fifth Fco_2 (Fco_2 = 0.12 and 0.98 respectively), the ISSM S_w decreased to 0.615. At Fco_2 of 1.0, a total of 1,084 PV of equilibrated $scCO_2$ was injected before full steady state was reached resulting in an ISSM S_w value of 0.328.

The $scCO_2$ flow rate during the bump flood was the same as the brine bump flow rate used in imbibition (10 ml/min). A total of 1,583 PV of equilibrated $scCO_2$ was required to achieve stability in both the differential pressure and ISSM data. The irreducible ISSM water saturation was 0.261.

The secondary imbibition results are presented in Table 5, **Fig. 11** and **Fig. 12**. The results are similar to those of the imbibition test showing a considerable spontaneous brine imbibition at the first water fractional flow of 0.025 (water flow rate of 0.2 ml/min) resulting in ISSM S_w of 0.555. From the second to the fifth F_w (F_w =0.15 and 0.96) respectively, the ISSM S_w increased to 0.619. Thus, the injection of both mutually equilibrated $scCO_2$ and brine from F_w of 0.025 to 0.96 resulted in a $scCO_2$ capillary trapping, Sco_{2r} of 0.381 FPV.

Table 3. Summary of injection rates, water fractional flow and measured imbibition relative permeability data.

Injection rate			Sw			Start	End	Prod.		
water	gas	Fw	ISSM	krw	kr_{CO_2}	time	time	ISSM	Injected volume	
(ml/min)	(ml/min)		(frac.)			(days)	(days)	(ml)	(ml)	(PV)
		0.000	0.229	0.000	1.000					
0.160	7.840	0.020	0.562	0.009	0.049	0.0	0.7	5.29	166	10
0.720	7.280	0.090	0.597	0.010	0.012	0.7	1.8	5.84	1117	70
1.200	2.800	0.300	0.608	0.014	0.004	1.8	2.9	6.02	1970	124
3.000	1.000	0.750	0.626	0.022	0.001	2.9	3.9	6.30	4167	262
3.760	0.240	0.940	0.629	0.024	0.000	3.9	4.8	6.34	5050	318
3.960	0.040	0.990	0.634	0.025	0.000	4.8	5.9	6.42	5853	369
4.000	0.000	1.000	1.001	0.483	0.000	5.9	11.8	12.25	34384	2166
10.000	0.000	1.000	1.008	0.483	0.000	11.8	12.7	12.37	13150	828

Table 4. Summary of injection rates, $scCO_2$ (gas) fractional flow and measured secondary drainage relative permeability data.

Injection rate			Sw			Start	End	Prod.		
gas	water	Fg	ISSM	kr_{CO_2}	krw	time	time	ISSM	Injected volume	
(ml/min)	(ml/min)		(frac.)			(days)	(days)	(ml)	(ml)	(PV)
		0.000	1.005	0.000	1.000					
0.060	3.940	0.015	0.688	0.000	0.055	0.0	3.7	5.03	320	20
0.480	3.520	0.120	0.684	0.001	0.057	3.7	4.7	5.09	679	43
1.600	2.400	0.400	0.683	0.004	0.055	4.7	5.7	5.11	2342	148
3.200	0.800	0.800	0.666	0.019	0.041	5.7	6.7	5.38	4422	279
3.920	0.080	0.980	0.615	0.098	0.017	6.7	8.0	6.19	7421	467
4.000	0.000	1.000	0.328	1.005	0.000	7.982	11.0	10.75	17212	1084
10.000	0.000	1.000	0.261	1.009	0.000	11.0	12.7	11.81	25136	1583

Table 5. Summary of injection rates, water fractional flow and measured secondary imbibition relative permeability data.

Injection rate			Sw			Start	End	Prod.		
water	gas	Fw	ISSM	krw	kr_{CO_2}	time	time	ISSM	Injected volume	
(ml/min)	(ml/min)		(frac.)			(days)	(days)	(ml)	(ml)	(PV)
		0.000	0.235	0.000	1.000					
0.200	7.800	0.025	0.555	0.010	0.045	0.0	2.8	5.08	809	51
1.200	6.800	0.150	0.592	0.019	0.012	2.8	3.9	5.67	1938	122
2.250	2.750	0.450	0.604	0.027	0.004	3.9	4.9	5.85	3208	202
3.900	1.100	0.780	0.617	0.035	0.001	4.9	6.9	6.06	11127	701
4.800	0.200	0.960	0.619	0.040	0.000	6.9	8.6	6.10	11842	746
5.000	0.000	1.000	1.003	0.692	0.000	8.6	15.2	12.19	47460	2989
10.000	0.000	1.000	1.006	0.692	0.000	15.2	16.8	12.24	22400	1411

Similar to the imbibition test, the S_{CO_2r} remained the same after injecting 10 PV of brine at $F_w = 1.0$ although full steady-state stability had not yet been obtained. In total, 2,989 PV of brine injection was required to achieve stability in both the pressure and ISSM data at $F_w = 1.0$ and progressively stripped the trapped $scCO_2$.

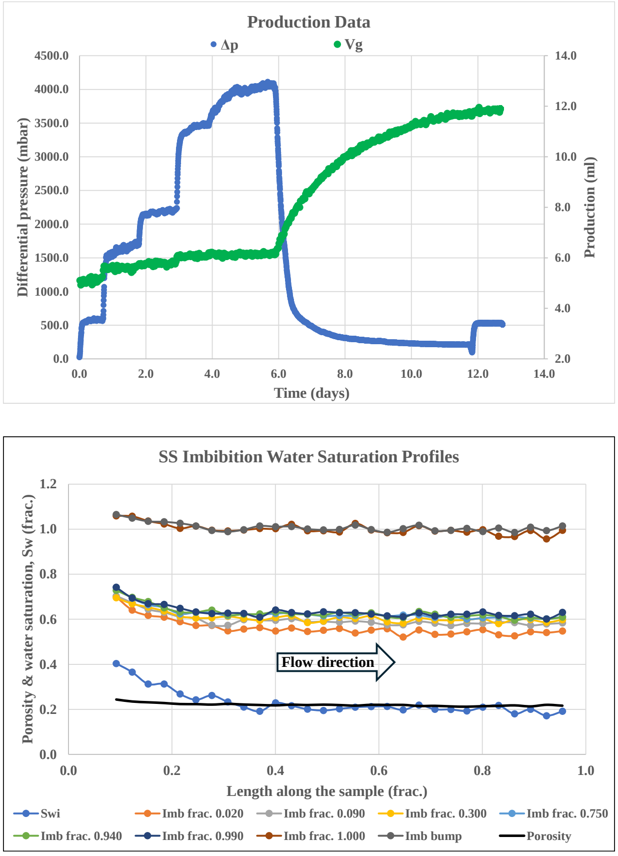

Fig. 7. Measured imbibition production data (top) and saturation profiles (bottom).

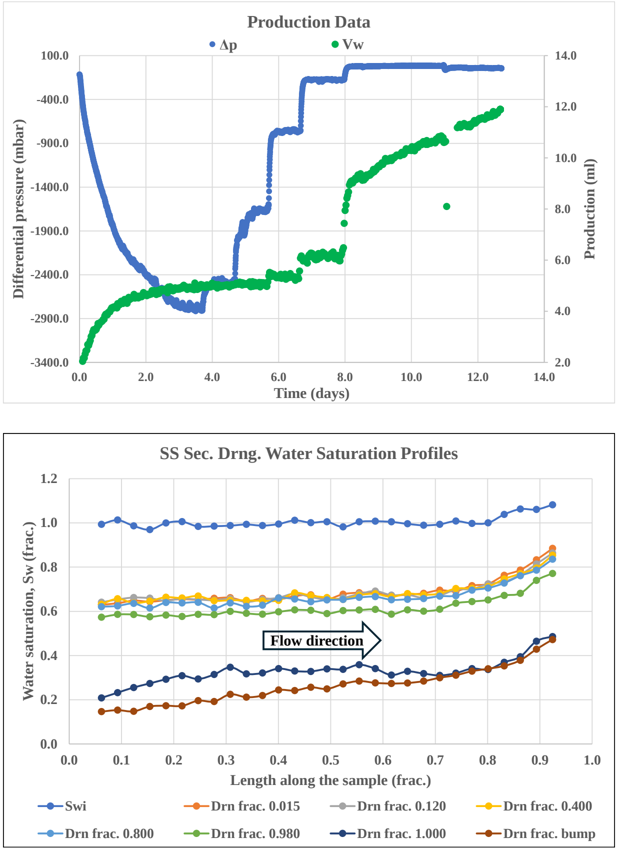

Fig. 9. Measured secondary drainage production data (top) and saturation profiles (bottom).

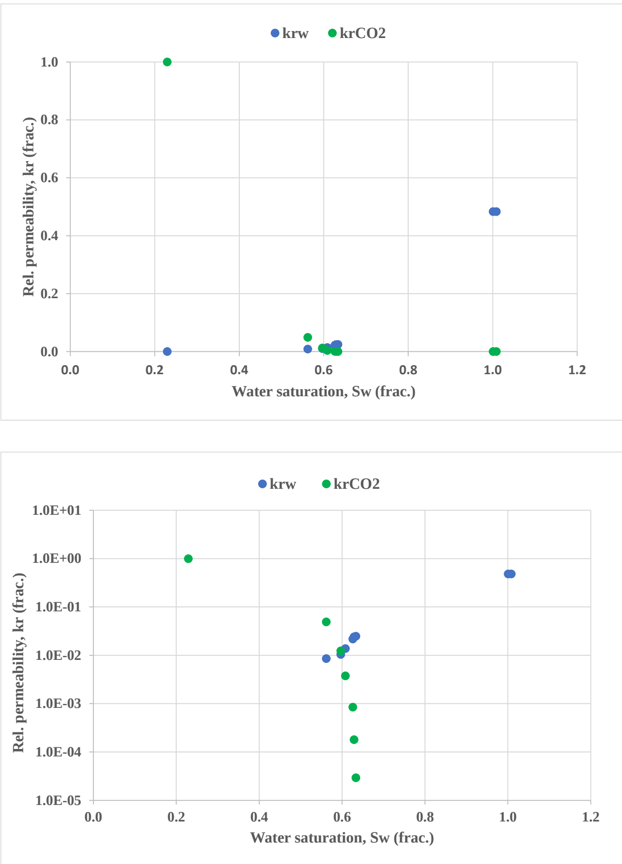

Fig. 8. Measured imbibition relative permeability curves: linear (top) and semi-log (bottom).

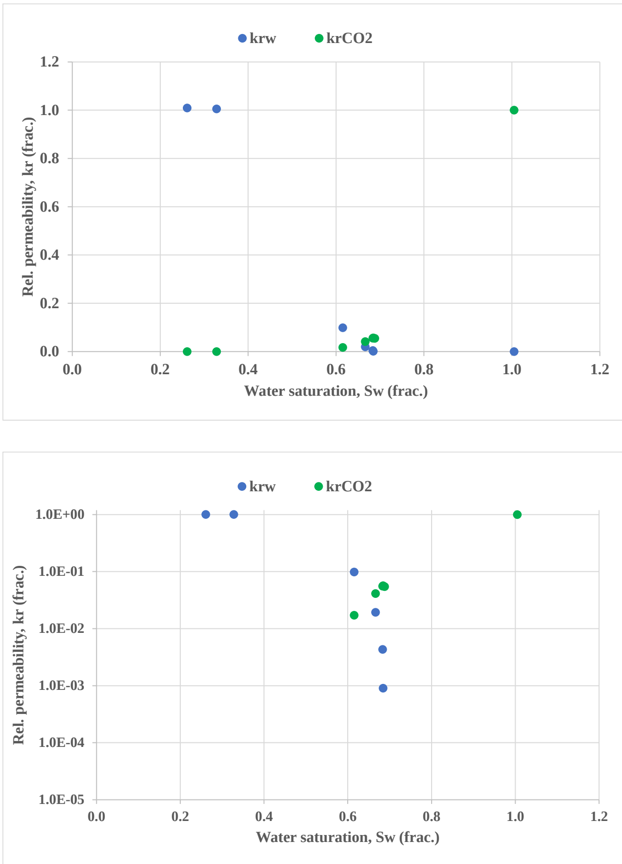

Fig. 10. Measured secondary drainage relative permeability curves: linear (top) and semi-log (bottom)

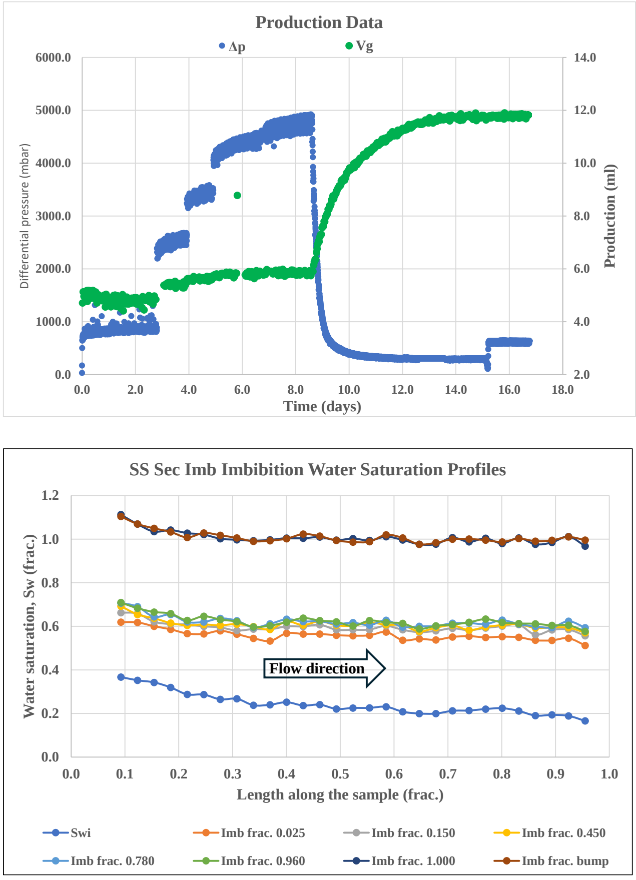

Fig. 11. Measured secondary imbibition production data (top) and saturation profiles (bottom).

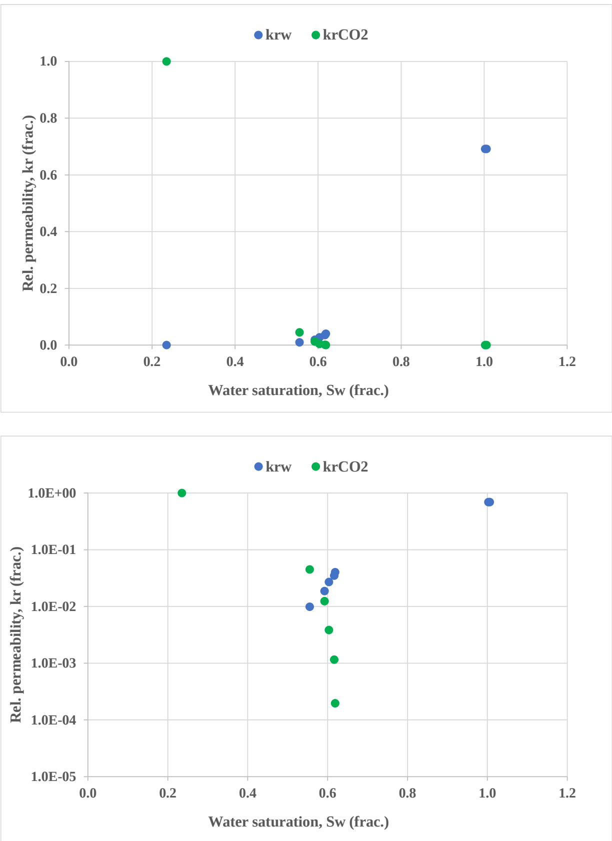

Fig. 12. Measured secondary imbibition relative permeability curves: linear (top) and semi-log (bottom).

3.3 Simulations and discussion of results

The porosity distribution along the core length is uniform as depicted in **Fig. 7** and confirms the relative homogeneity observed in the CT scan Sample #1 - **Fig. 3**. Establishment of the S_{wi} using the porous plate method ensures a good desaturation of the cores with minimal end effects as shown by the S_{wi} profiles in **Fig. 7**. Since the cores were cleaned and dried as described in subsection 2.1 and were not exposed to crude oil, they were expected to be water wet. The imbibition results can be divided into two parts as follows.

3.3.1 Imbibition results – Part A: injection of both $scCO_2$ and brine

The simultaneous injection of both equilibrated $scCO_2$ and brine can be likened to the upward migration of injected $scCO_2$ and downward migration of brine due to buoyancy forces at the end of scCO2 injection into saline aquifers.

At the first $F_w = 0.02$, the imbibition results showed a considerable spontaneous imbibition of 0.333 saturation units (s.u.) of brine, and the average water saturation increased to 0.562 - **Fig. 7**.

Idowu et al. [17] presented similar results of a substantial spontaneous water imbibition with water displacing oil from smaller pores and near grain surfaces due to capillarity with large blobs of oil as residual in pore bodies due to snap-off effects in the pore throats for a water-wet homogeneous outcrop sample - **Fig. 13**.

Increasing the F_w from the second to the sixth (F_w = 0.09 and 0.99 respectively) only resulted in additional displacement of 0.071 s.u. of $scCO_2$. Also, no further brine imbibition was observed even after injecting 10 PV of brine at F_w = 1.0 and the endpoint water relatively permeability was 0.025.

Results presented in [17] also demonstrated that the presence of clay minerals such as grain lining clays aid retention of water and water-wetness to cause oil snap-off. As stated in subsection 2.1, the cores contained approximately 5 wt% of clay minerals – illite, mica, kaolinite, etc - **Fig. 4**. These possibly grain lining clays may have contributed to 0.366 FPV of capillary trapped $scCO_2$ during the co-injection of both $scCO_2$ and brine.

The measured production and pressure data from this part (Part A) was history matched using a two-phase core flow simulator. **Fig. 14** and **Fig. 15** compare the simulated and experimental data and show a very good agreement. The measured and simulated trapped $scCO_2$ and water relative permeability endpoints were 0.366 and 0.352 FPV and; 0.025 and 0.027 respectively.

These experimental and simulated results confirm that the core sample was strongly water wet, the residual scCO2 was trapped by capillary forces, and demonstrate the suitability of Ivar Aasen field as a CCS analogue with a capillary trapping of ≈ 0.36 FPV. This translates to a trapping efficiency of ≈ 47.47% of the initial $scCO_2$ saturation!

Besides this very good capillary trapping efficiency, evaluation and assessment of Ivar Aasen sandstone cores for the other three trapping mechanisms will further reinforce its suitability as a CCS analogue.

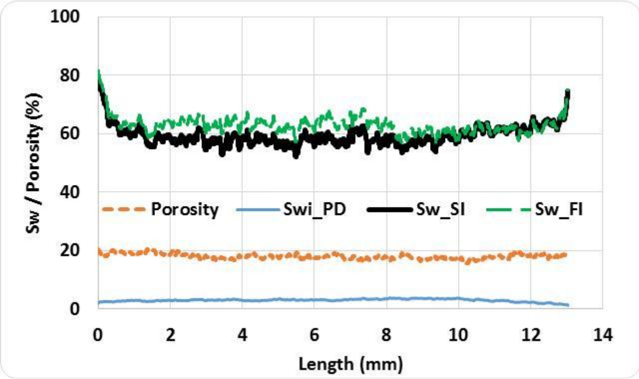

Fig. 13. Longitudinal profiles of porosity (% bulk volume) and S_w (% PV) after primary drainage, spontaneous and forced imbibition, for the miniplugs of the homogeneous outcrop Sample [17].

3.3.2 Imbibition results – Part B: injection of only equilibrated brine.

At F_w = 1.0 and during the bump flow, only equilibrated brine was injected. It took 6 days and injection of 2,166 PV of equilibrated brine before full steady-state stability was reached in pressure and production data. This excessive brine throughput progressively stripped the trapped $scCO_2$ resulting in S_w = 1.0 even though the $scCO_2$ and the brine were mutually equilibrated. This is a laboratory artefact and not feasible in reality.

Hence, there was no point simulating this part of the imbibition results. The solubility of $scCO_2$ in brine depends largely on pressure, temperature and equilibration time. While the time requires to achieve a good equilibration may range from few days to weeks [18], it has been demonstrated “that even closely equilibrated fluids can still exhibit degree of evaporation/dissolution that can impact in situ fluid distribution” - [20].

For the bump flow at 10 ml/min, steady-state stability was reached after 0.9 days, and the water saturation value remained the same (S_w = 1.0). The capillary number (equation 1) was N_c = 8.92E-07 and N_c = 2.23E-06 at F_w = 1.0 and bump flood respectively confirming that the measurements were capillary dominated.

$$N_c = \frac{k_{rw} \times K \times \Delta P}{L \times \sigma} \qquad (1)$$

3.3.3 Secondary drainage results

Injection of $scCO_2$ (non-wetting phase) at the end of the imbibition process was experimentally a secondary drainage process and the pressure/production data, saturation profiles and measured relative permeability are depicted in Table 4, **Fig. 9** and **Fig. 10**. However, since the S_w = 1.0 at the beginning of the test, this test may technically be considered as a primary drainage test.

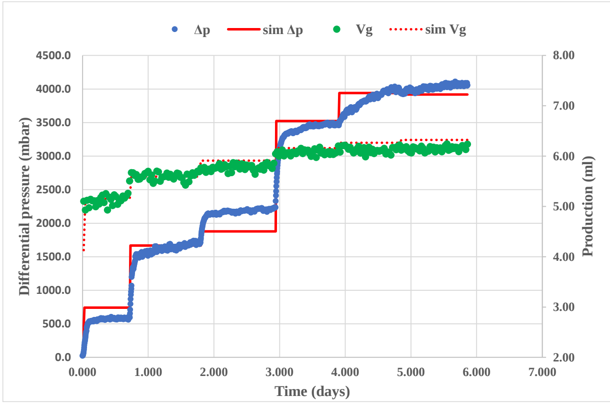

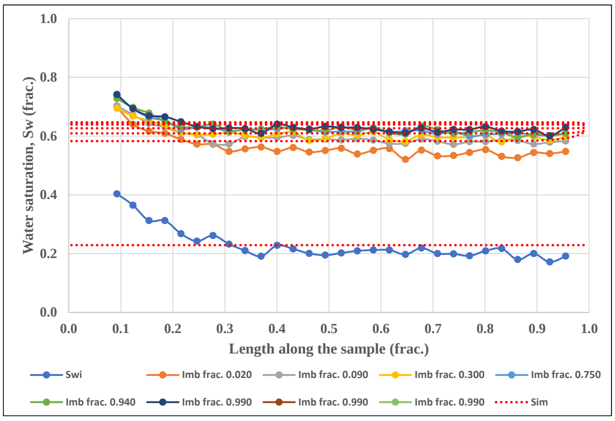

Fig. 14. Measured and simulated imbibition saturation profiles.

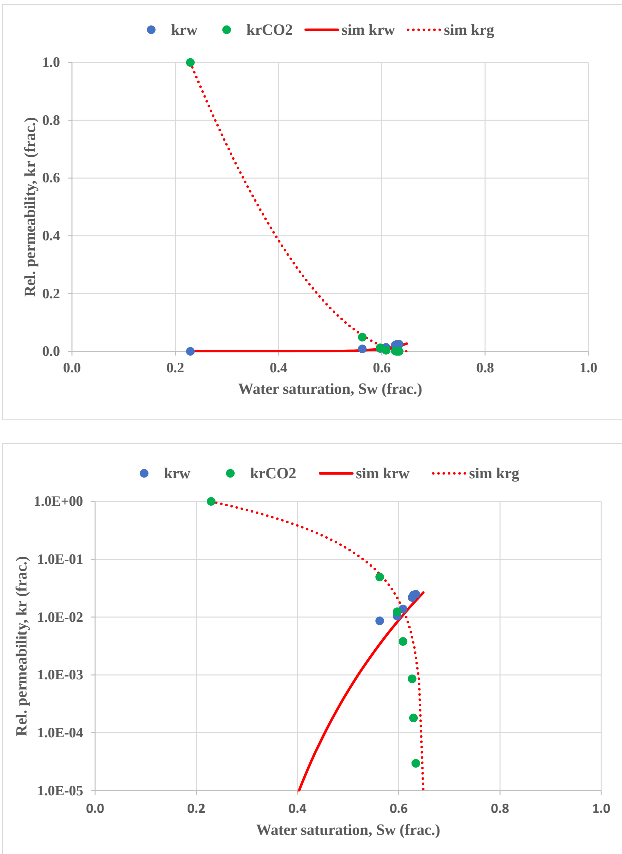

Fig. 15. Measured and simulated imbibition relative permeability curves: linear (top) and semi-log (bottom).

At the first Fco_2 = 0.015 ($scCO_2$ flow rate of 0.06 ml/min), the injected $scCO_2$ progressively invaded the largest available pores/throats and the differential pressure increased as the available pores/throats sizes decreased. It took 3.7 days (20.5 PV) to reach full steady-state stability.

For strongly wetting systems, primary drainage results should mirror the imbibition results and vice versa. Accordingly, increasing the $scCO_2$ fractional flow from the second to the fifth step (Fco_2 = 0.12 and 0.98 respectively) resulted in an additional displacement of only 0.073 s.u. of equilibrated brine, which is nearly identical to the imbibition test where 0.071 s.u. of $scCO_2$ was displaced by increasing the F_w from the second to the sixth water fractional flow step (F_w = 0.02 to 0.99). Injection of only $scCO_2$ at Fco_2 = 1.0 and during the bump flood, resulted in additional displacements of equilibrated brine by 0.287 and 0.067 s.u. respectively.

A comparison of the saturation profiles at the end of the imbibition F_w = 0.99 and at the end of the drainage Fco_2 = 0.98 shown in **Fig. 16** further corroborates the mirror-image relationship between the two tests and the strongly wetting behaviour of the system. Fco2 = 0.98 corresponds to F_w = 0.02 and exhibits saturation profiles that are nearly identical to those observed at F_w = 0.99 during the imbibition test.

However, the irreducible water saturation at the end of the drainage bump flood (S_{wirr} = 0.261) is higher than the S_{wi} = 0.229 calculated at the beginning of the imbibition tests. The difference of 0.032 s.u. might be due to the difference in the applied maximum capillary pressure during the gas/brine porous plate and the steady-state drainage tests. Hence, hysteresis analysis between the imbibition and the secondary/primary drainage is not feasible due to this difference. The S_{wirr} profiles are also less uniformly distributed than the porous plate S_{wi} profiles - **Fig. 16**.

3.3.4 Secondary imbibition results

The water saturation at the end of the imbibition and at the beginning of the secondary drainage measurements were 1.008 and 1.005 respectively. Although the flow direction changed from bottom-to-top for the imbibition test to top-to-bottom for the drainage test, $S_w \approx$ 1.0 because the core remained fully saturated with brine – **Fig. 7** and **Fig. 9**.

However, at the end of the drainage tests, the plug sample was saturated with both scCO2 and equilibrated brine (S_{wirr} = 0.261). Changing the flow direction from to top-to-bottom for the drainage test to bottom-to-top for the secondary imbibition test (to ensure gravity stable injection/displacement) resulted in redistribution of the fluids and an additional brine drainage of 0.026 s.u. during the base permeability measurement $kco_2(S_{wirr})$ for the secondary imbibition test – **Fig. 16**.

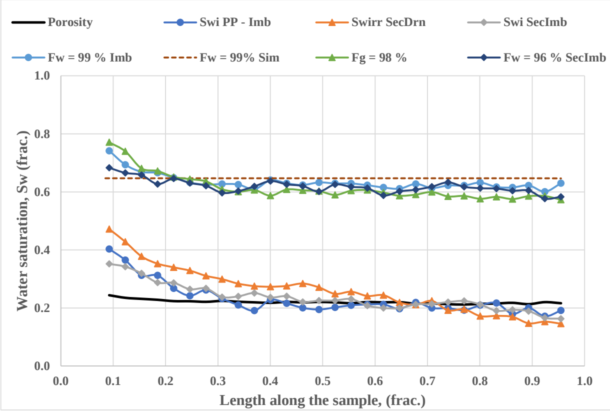

Fig. 16. Porosity profiles, porous plate water saturation profiles at the beginning of the imbibition tests, end of the secondary drainage test, beginning of the secondary imbibition, imbibition F_w = 99%, simulated Fw = 99%, secondary drainage Fg = 98% and secondary imbibition F_w = 96%.

Thus, at the beginning of the secondary imbibition test, the initial water saturation, S_{wi} = 0.235. To maintain consistent S_w values between the end of the secondary drainage and the beginning of secondary imbibition, we recommend using the same flow direction (bottom to top) for all measurements, including imbibition, secondary drainage and secondary imbibition in future experiments. Interestingly, the resulting S_{wi} = 0.235 is not only comparable to S_{wi} = 0.229 at the beginning of the first imbibition but also shows similar saturation profiles **Fig. 16**.

Since the secondary drainage could technically be considered as a primary drainage test, the subsequent secondary imbibition can likewise be interpreted as an imbibition test. It is therefore not surprising that the results from this test closely replicate those obtained from the first imbibition experiment as shown in **Fig. 16** and **Fig. 17**. The measured water saturation profiles and relative permeability curves are almost indistinguishable and show good agreement with the simulated data.

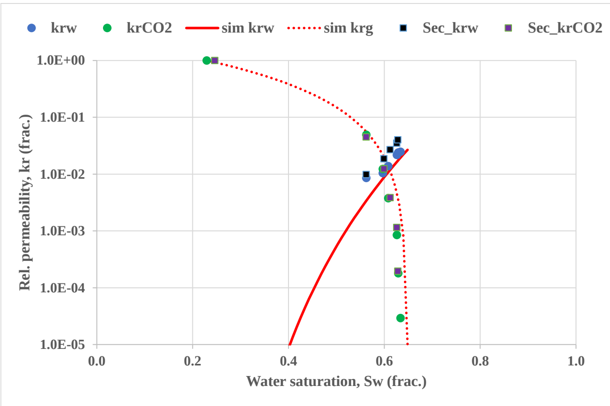

Fig. 17. Comparison of measured first imbibition, simulated and measured secondary imbibition relative permeability curves: semi-log.

Similarly, the Sco_{2r} remained the same after injecting 10 PV of brine at F_w = 1.0 although full steady-state stability had not yet been obtained. To prevent stripping and preserve physically meaningful residual trapping, we argue that stability in the differential pressure and ISSM data is not a necessary criterion at $F_w = 1.0$ and during the bump flood. Consequently, we recommend limiting the total pore volume of brine injected to a maximum of 5 PV in future similar experiments. This threshold corresponds to 50% of 10 PV of brine injected before the onset of stripping was observed during the imbibition tests.

The most widely used trapping and relative permeability model is the Land correlation [19]. In this model, the capillary trapped gas saturation (S_{gt}) after imbibition is a function of the initial gas saturation (S_{gi}) obtained at the end of the primary drainage – equation 2. The Land coefficient, C can be calculated from the experimental and or simulated S_{gi} and S_{gt} using equation 3.

$$S_{gt} = \frac{S_{gi}}{1 + CS_{gi}} \qquad (2)$$

$$C = \frac{1}{S_{gt}} - \frac{1}{S_{gi}} \qquad (3)$$

Fig. 18 depicts the measured/simulated trapped gas saturations together with the calculated Land correlation C-coefficients while Table 6 summarizes the first imbibition, simulation and secondary imbibition results and shows good agreement.

One of the challenges of steady state measurements is the potential saturation inaccuracies due to disequilibria effects [18]. By ensuring that the dP values were maintained below 5% of the pore pressure throughout the tests, the water saturation profiles for imbibition and secondary imbibition are (fairly) uniform from the first to the last water fractional flow steps - **Fig. 7** and **Fig. 11**. However, slight capillary end effects were observed in the secondary drainage water saturation profiles as depicted in **Fig. 9**.

Obtaining trapped CO_2 saturation and endpoint brine relative permeability at reservoir conditions with unsteady state low-rate waterflooding is cheaper and faster for saline aquifers but may be unsuitable for depleted oil and gas reservoirs due to wettability issues [7]. Hence, properly conducted steady state experiments with appropriate equipment and experienced staff are recommended. The measured production and pressure data as well as relative permeability curves should also be history matched.

The accuracy of the γ-ray ISSM saturation values depends largely on the equilibrated brine and $scCO_2$ reference or calibration scans acquired at the end of the secondary imbibition tests. The γ-ray intensity is a function of rock attenuation and the in-situ brine and $scCO_2$ attenuation. Using these calibration scans allows the intermediate saturations to be quantified.

It was therefore very important to ensure that the plug sample was properly cleaned after KF titration and fully re-saturated with brine before acquiring brine reference scans. Similarly, the core was dried by using critical point drying and subsequently reflooded with $scCO_2$ before the acquisition of $scCO_2$ reference scans.

Besides, fluid saturations were computed from 0.092 to 0.955 length fraction of the sample to remove end-effects from the, γ-ray ISSM data. For these measurements, the uncertainty in the ISSM saturation values is estimated to be +/- 1.0%.

3.3.5 Saturation control results

Karl Fischer (KF) titration is a standardised procedure for determination of water volumes contained within a fluid sample. The water content from the KF titration was 15.33 ml at the end of the secondary imbibition tests. This translates to $S_w = 0.964$ based on the test pore volume of 15.88 ml. This is 0.036 s.u. less than expected since all the trapped scCO2 have been stripped progressively by the excessive injection of equilibrated brine. This difference is within the acceptable experimental errors of less than 0.05 s.u. and might be due to not being able to displace all the water in the plug during the KF procedure.

Table 6. Summary of imbibition, simulation and secondary imbibition results.

	Imbibition	Simulation	Secondary imbibition
S_{wi}	0.229	0.229	0.235
$scCO_{2i}$	0.771	0.771	0.765
$scCO_{2t}$	0.366	0.352	0.381
Trapping efficiency	47.5%	45.7%	49.8%
Kw^*	0.025	0.027	0.040
Land coefficient	1.432	1.544	1.317

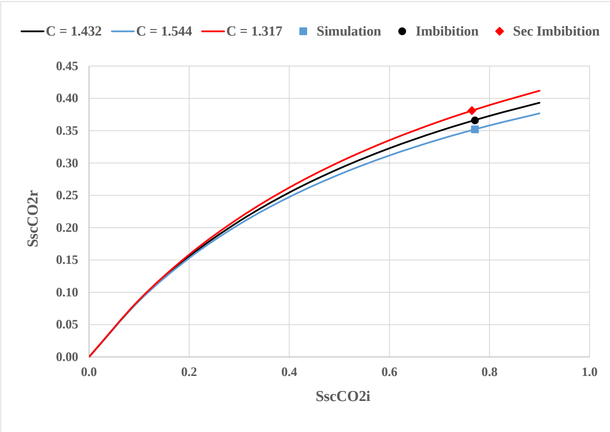

Fig. 18. Trapped $scCO_{2r}$ vs. initial $scCO_{2i}$ with calculated Land correlation coefficients

3 Conclusions and recommendations

Based on the results of these measurements, the following conclusions and recommendations are given:

- The core sample was strongly water wet with a capillary trapping of 0.36 – 0.38 FPV.
- The suitability of Ivar Aasen field as a CCS analogue with a trapping efficiency of more than 47 % of the initial scCO2 saturation.
- The simulated data shows a very good agreement with the measured imbibition data and reinforces

the suitability of Ivar Aasen field as a CCS analogue.

- The total pore volume of brine injected during imbibition test at $F_w = 1.0$ as well as during the bump flood should be limited to a maximum of 5 PV. This is to prevent stripping and preserve physically meaningful residuals in future similar experiments.
- To ensure consistent water saturation at the end of one test (e.g. imbibition) and at the beginning of the next measurement (e.g. secondary drainage) for hysteresis analysis, the same flow direction should be maintained across all stages of the experiment.
- Cores should be properly cleaned and re-saturated fully before acquisition of the equilibrated fluids reference scans to reduce uncertainties in the calculated ISSM saturation values to < 1.0%.
- For cores containing clay minerals, gentle cleaning and drying procedures should be employed to preserve the integrity of the clay structure and prevent alteration of mineralogy or pore-scale properties.

Acknowledgments

The authors acknowledge Stratum Reservoir Norway and AkerBP for granting permission to publish this paper. This study was part of the Norwegian Carbon Capture and Storage (NCCS) Research with the aim of facilitating large-scale geological storage of CO_2 through industry-driven innovation.

References

1. S. Bachu. Drainage and imbibition CO_2/brine relative permeability curves at in situ conditions for sandstone formations in western Canada. Energy Procedia, **37**, 4428 – 4436, (2013)
2. S.A. Mathias, J.G. Gluyasa, G.J. González Martínez de Miguela, S.L. Bryantc, D. Wilson. On the importance of relative permeability data for estimating CO_2 injectivity in brine aquifers. Int. J. of Greenhouse Gas Control, 1**2**, 200 – 212, (2013)
3. J.-C. Perrin, M. Krause, C.-W. Kuo, L. Miljkovic, E. Charoba, S. M. Benson. Core-scale experimental study of relative permeability properties of CO_2 and brine in reservoir rocks. Energy Procedia, 1, 3515 - 3522, (2009)
4. C.-W. Kuo, J.-C. Perrin, S. M. Benson. Effect of gravity, flow Rate, and small scale heterogeneity on multiphase flow of CO_2 and brine. *SPE Western Regional Meeting*, SPE-132607, (2010)
5. J.-C. Perrin, S. M. Benson. An Experimental Study on the Influence of Sub-Core Scale Heterogeneities on CO_2 Distribution in Reservoir Rocks. Trans. in Porous Media, **82**, 93 - 109, (2010)
6. N. M. Burnside, M. Naylor. Review and implications of relative permeability of CO_2/brine systems and residual trapping of CO_2. Int. J. Greenhouse Gas Control, **23**, 1 - 11, (2014)
7. E. Ebeltoft, M. Recordon, R. Meneguolo, J.G. Jacobsen, R. Askarinezhad, R. Pitman. SCAL model for CCS – Insights from the first commercial CO_2 project on the Norwegian Continental Shelf, Northern Lights. SCA2023-016, (2023)
8. R. Askarinezhad, J. O. Helland, J. C. Zuta. Automated History Matching of Steady-State CO_2/Brine Drainage Experiments at Reservoir Conditions. SPE-231939, (2026)
9. B. Bennion, S. Bachu. Relative permeability characteristics for CO_2 displacing water in a variety of potential sequestration zones in the Western Canada Sedimentary Basin. In SPE Annual Technical Conference and Exhibition, SPE-95547 MS (2005)
10. B. Bennion, S. Bachu. Drainage and imbibition relative permeability relationships for supercritical CO_2/brine and H_2S/brine. SPE Res. E. & Eng., **11**, 487-96, (2008)
11. B. Bennion, S. Bachu. Drainage and Imbibition CO2/Brine Relative Permeability Curves at Reservoir Conditions for Carbonate Formations. In SPE Annual Technical Conference and Exhibition SPE-134028 (2010)
12. M.N.A. Akbar, B. Jenei, M. Lakos, B. Steffens, S. Kulaksiz, L. Ganzer. Assessing the Impact of Relative Permeability Uncertainty on Geological CO2 Storage Using SCAL Modeling and Numerical Simulation. SPE-231936, (2026)
13. O. Massarweh, A.S. Abushaikha. CO_2 sequestration in subsurface geological formations: A review of trapping mechanisms and monitoring techniques. Earth-Science Rev, **253** (2024) 104793
14. Intergovernmental Panel on Climate Change, (2008)
15. https://okea.no/wp-content/uploads/2026/03/OKEA-ASA-Annual-Statement-of-reserves-and-resources-2025.pdf
16. Https://en.wikipedia.org/wiki/Supercritical_carbon_dioxide
17. N. Idowu, H. Long, P.E. Øren, A.M. Carnerup, A. Fogden, I. Bondino, L. Sundal. Wettability analysis using micro-CT, FESEM and QEMSCAN, and its applications to digital rock physics SCA2015-010, (2015)
18. A. Cense, J. Reed, P. Egermann. SCAL for gas reservoirs : a contribution for better experiments. SCA2016-023, (2016)
19. C. Land. Comparison of Calculated with Experimental Imbibition Relative Permeability. SPE J., **11**, 419-425, (1971)
20. D. Magzymov, G. Jerauld, L. Lun, J. Golias, K. Vidal, A. Foernes, T. Danielsen. Evidence of Water-Wet Behavior for Supercritical CO2: Drainage and Imbibition Capillary Pressure Measurements Using the Semi-Dynamic Method. In SPE Annual Technical Conference and Exhibition, SPE-227909, (2025)